



1 Evaluation of the Aqua MODIS Collection 6.1 multilayer cloud detection algorithm through
2 comparisons with CloudSat CPR and CALIPSO CALIOP products

3

4 Benjamin Marchant^{1,2}, Steven Platnick¹, Kerry Meyer¹, and Galina Wind^{1,3}

5 1: NASA Goddard Space Flight Center; 2: USRA Universities Space Research Association; 3:

6 SSAI: Science Systems and Applications, Inc.

7 benjamin.marchant@nasa.gov

8

9 **Abstract:**

10

11 Since multilayer cloud scenes are common in the atmosphere and can be an important
12 source of uncertainty in passive satellite sensor cloud retrievals, the MODIS MOD06/MYD06
13 standard cloud optical property products include a multilayer cloud detection algorithm to assist
14 with data quality assessment. This paper presents an evaluation of the Aqua MODIS MYD06
15 Collection 6.1 (C6.1) multilayer cloud detection algorithm through comparisons with active CPR
16 and CALIOP products that have the ability to provide cloud vertical distributions and directly
17 classify multilayer cloud scenes and layer properties. To compare active sensor products with an
18 imager such as MODIS, it is first necessary to define multilayer clouds in the context of their
19 radiative impact on cloud retrievals. Three main parameters have thus been considered in this
20 evaluation: (1) the maximum separation distance between two cloud layers, (2) the
21 thermodynamic phase of those layers, and (3) the upper layer cloud optical thickness. The impact
22 of including the Pavolonis-Heidinger multilayer cloud detection algorithm, introduced in Collection
23 6, to assist with multilayer cloud detection has also been assessed. For the year 2008, the MYD06
24 C6.1 multilayer cloud detection algorithm identifies roughly 20 percent of all cloudy pixels as



25 multilayer (decreasing to about 13 percent if the Pavolonis-Heidinger algorithm output is not
26 used). Evaluation against the merged CPR and CALIOP 2B-CLDCLASS-lidar product shows that
27 the MODIS multilayer detection results are quite sensitive to how multilayer clouds are defined in
28 the radar/lidar product, and that the algorithm performs better when the optical thickness of the
29 upper cloud layer is greater than about 1.2 with a minimum layer separation distance of 1km.
30 Finally, we find that filtering the MYD06 cloud optical properties retrievals using the multilayer
31 cloud flag improves aggregated statistics, particularly for ice cloud effective radius.

32

33 **I - Introduction**

34

35 Detection of multilayer clouds using passive sensors such as the Moderate-resolution
36 Imaging Spectroradiometer (MODIS) is a challenging but important remote sensing need. The
37 existence of multiple cloud layers may strongly impact retrievals of cloud optical, microphysical,
38 and cloud-top properties under single layer plane-parallel cloud assumptions. For example, the
39 MODIS Collection 6/6.1 (C6/C6.1) cloud optical property retrievals (MOD06/MYD06 for
40 Terra/Aqua, respectively), which assume a homogeneous plane-parallel cloud model as did
41 previous collections (Platnick et al. 2017), have been shown to have significant microphysical
42 cloud retrieval errors or outright failures for pixels that are identified as multilayer. As such, a
43 multilayer cloud detection algorithm (Wind et al. 2010) was first developed for Collection 5 as a
44 quality assurance metric to identify multilayer cloudy scenes. The MYD06 multilayer cloud flag
45 has subsequently been used synergistically with optical centroid cloud pressure derived from
46 Ozone Monitoring Instrument (OMI) UV observations to further identify multilayer and vertically
47 extended clouds (Joiner et al. 2010). Beyond MODIS, other passive multilayer cloud detection
48 techniques use polarized reflectances, such as those from the Polarization and Directionality of
49 the Earth's Reflectance (POLDER) instrument (Desmons et al, 2017), in addition to spectral



50 signature differences between monolayer and multilayer cloud scenes determined from forward
51 radiative transfer models (Pavolonis and Heidinger, 2004; Heidinger and Pavolonis, 2005; Nasiri
52 and Baum, 2004; Jin and Rossow, 1997). Several studies have also been dedicated to the
53 inference of cloud optical properties for multilayer cloud scenes, e.g., Watts et al. (2011),
54 Sourdeval et al. (2014) and Chang and Li (2005). Those studies use a two-layer cloud overlapping
55 model approximation coupled with, e.g., optimal estimation, to derive the cloud optical properties
56 associated with the two cloud layers, and thus inherently require robust multilayer cloud detection.
57

58 Evaluating the performance of multilayer cloud detection algorithms requires appropriate
59 truth datasets and an understanding of the intent of the algorithm itself. For instance, the
60 MOD06/MYD06 multilayer cloud detection algorithm was initially evaluated using forward
61 radiative transfer simulations (Wind et al., 2010), though these cannot fully capture the complexity
62 of the real atmosphere. Active sensors, on the other hand, such as the CloudSat Cloud Profiling
63 Radar (CPR) and the Cloud-Aerosol Lidar with Orthogonal Polarization (CALIOP) onboard the
64 Cloud-Aerosol Lidar and Infrared Pathfinder Satellite Observation (CALIPSO) satellite, both in the
65 afternoon “A-train” constellation, provide key details on cloud vertical structure. Merged
66 CPR/CALIOP products that exploit the different yet complementary sensitivities of radar and lidar
67 observations have demonstrated utility for evaluating passive multilayer cloud detection
68 algorithms. In fact, the MOD06/MYD06 multilayer cloud flag previously has been evaluated by
69 Wang et al. (2016) using the 2B-CLDCLASS-LIDAR product for the years 2007-2010, and by
70 Desmons et al. (2017), who in parallel evaluated the PARASOL-POLDER multilayer cloud
71 detection algorithm using the 2B-GEOPROF-lidar and CALIOP 5km cloud layer products for the
72 years 2006-2010. These investigations, however, broadly defined multilayer clouds in the
73 radar/lidar datasets and thus implicitly did not consider the intent of the MOD06/MYD06 multilayer
74 cloud detection algorithm, which is to identify scenes where a second cloud layer adversely



75 impacts the optical property retrievals of the radiatively dominant cloud layer (the primary example
76 being a thin ice cloud overlying an optically thicker liquid water cloud), rather than as a strict
77 multilayer detection algorithm. For example, Desmons et al. defined a multilayer cloud when CPR
78 and CALIOP detected two spatially distinct cloud layers, regardless of the separation distance
79 between the cloud layers and cloud thermodynamic phase, while Wang et al. specified only that
80 detected cloud layers must be separated vertically by at least 480m to be considered multilayer.
81

82 In this paper, the main purpose is to present an evaluation of the Aqua MODIS (MYD06)
83 C6.1 multilayer cloud detection algorithm through comparisons with CPR and CALIOP merged
84 products. In addition, we will investigate how multilayer clouds affect MYD06 cloud
85 thermodynamic phase results which have strong consequences for microphysical retrievals. In
86 the first section we provide a short overview of the MOD06/MYD06 multilayer cloud detection
87 algorithm. The second section provides details about the datasets and the methodology used for
88 the evaluation. The third section presents evaluation results as a function of three main
89 parameters used to define a multilayer cloud scene in the CPR/CALIOP merged products: (1) the
90 separation distance d between the two radiatively dominant cloud layers, (2) the thermodynamic
91 phase of those layers, and (3) the layer optical thicknesses, in particular of the upper cloud layer.
92 Finally, in the last section, we show the impact of multilayer clouds on cloud effective radius
93 retrievals.

94

95 **III – The MOD06/MYD06 multilayer cloud detection algorithm**

96

97 Originally introduced in Collection 5 (C5), the MOD06/MYD06 multilayer cloud detection
98 algorithm was developed as a quality assurance (QA) flag to identify scenes where the single-
99 layer cloud forward model assumption is likely violated. Its primary targets are those scenes



100 where an optically thinner cloud overlies an optically thicker liquid cloud, either where the phases
101 of the two layers differ (ice over liquid) or the vertical separation is sufficiently large such that
102 retrievals of the optical properties of the radiatively dominant underlying cloud are adversely
103 impacted. The algorithm operates on a pixel-level basis (1km resolution at nadir), with cumulative
104 results reported in the Cloud_Multi_Layer_Flag Science Data Set (SDS) in the MOD06/MYD06
105 Level-2 files and individual test results reported as bit values in the Quality_Assurance_1km SDS.
106 Full details on the C5 algorithm can be found in Wind et al. (2010); updates for C6/C6.1 are
107 summarized in Platnick et al. (2017) and the C6/C6.1 User's Guide (Platnick et al., 2018).

108

109 The algorithm is based primarily on four tests that are collectively used to classify a cloudy
110 pixel as monolayer or multilayer:

- 111 1. A cloud thermodynamic phase difference test, where divergent results between the IR
112 phase algorithm (Baum et al., 2012) and the shortwave/IR optical properties phase
113 algorithm (Marchant et al., 2016) yield a positive multilayer cloud result.
- 114 2. An above-cloud precipitable water (PW) difference test (ΔPW), using the relative difference
115 between above-cloud PW derived from the CO₂-slicing cloud-top pressure result and that
116 derived from the 0.94 μ m channel with respect to the total PW (TPW) derived from ancillary
117 atmospheric profiles; a relative difference larger than 8% yields a positive multilayer cloud
118 result.
- 119 3. A second above-cloud PW difference test (ΔPW_{900mb}), similar to the ΔPW test above but
120 assuming the cloud is located at 900mb when deriving above-cloud PW from the 0.94 μ m
121 channel; again, a relative difference of 8% yields a positive multilayer cloud result.
- 122 4. A test based on the algorithm of Pavolonis and Heidinger (2004) (hereafter referred to as
123 PH04 for brevity), introduced in C6, that uses reflectance at 0.65 μ m and 11 and 12 μ m



124 brightness temperatures and brightness temperature differences, in addition to
125 reflectances at 1.6 and 1.38 μm .

126

127 A test based on the divergence of cloud optical thickness retrievals from the standard VNSWIR
128 (Visible, near or shortwave infrared)-2.1 μm channel pair and the 1.6-2.1 μm channel pair was also
129 introduced in C6, but updates to the optical properties retrieval solution logic rendered this test
130 ineffective (see Platnick et al., 2018) and we do not consider it here. Note that the MOD06/MYD06
131 multilayer cloud algorithm is only applied to pixels having cloud optical thickness larger than 4.
132 Moreover, during algorithm development, the above tests, when positive, were assigned pre-
133 defined confidence values, the summation of which is reported in the Cloud_Multi_Layer_Flag
134 SDS and was intended to provide a pseudo-confidence level; a value of 0 indicates no cloud was
135 detected, 1 indicates a monolayer cloud, and values 2-10 indicate the cumulative weight of the
136 positive multilayer tests.

137

138 Figure 1 shows aggregated Aqua MODIS MYD06 Level 2 cloud products over the year 2008
139 (all data from C6.1 unless otherwise noted): (a) total cloud fraction from the MYD35 cloud mask
140 product after removing pixels identified as heavy aerosol or sun glint by the MYD06 clear sky
141 restoral (CSR) algorithm, (b) multilayer cloud fraction, (c) multilayer cloud fraction without the
142 PH04 test, and (d) C5.1 multilayer cloud fraction. The multilayer cloud fractions determined by
143 each individual C6/C6.1 multilayer cloud detection test are shown in the remaining panels: (e)
144 cloud phase difference test, (f) ΔPW test, (g) $\Delta\text{PW}_{900\text{mb}}$ test, and (h) PH04 test. Note that the
145 multilayer fraction shown in Fig. 1c uses a similar definition for multilayer clouds, i.e., excluding
146 the PH04 test, as does the MOD08/MYD08 C6/C6.1 Level-3 (L3) aggregated products; this test
147 was excluded during C6 L3 development after preliminary analysis indicated that it was overly
148 aggressive in some circumstances. For the year 2008, we find that about 20% of cloudy pixels



149 are flagged as multilayer clouds, a number that decreases to 13% if the PH04 test is excluded
150 (similar to MOD06/MYD06 C5 results, Fig. 1d). Considering the multilayer cloud fraction in Fig.
151 1b where all tests contribute to the results, we find that about 21% of all positive multilayer cloud
152 results have a positive cloud phase difference test, 28% have a positive ΔPW test, 44% have a
153 positive $\Delta PW_{900\text{mb}}$ test, and 74% have a positive PH04 test.

154

155 **III - Data Sets and Methodology**

156

157 We evaluate the MODIS C6.1 multilayer cloud detection algorithm using co-located A-Train
158 CloudSat CPR and CALIPSO CALIOP data during the year 2008. Due to its location in the A-
159 Train, only Aqua MODIS MYD06 data is used; note that the multilayer algorithm applied to Terra
160 MODIS is identical to that applied to Aqua MODIS. Rather than consider CPR data separately,
161 we use the 2B-CLDCLASS-lidar CPR-CALIOP merged product in addition to the CALIOP Version
162 4 5km cloud layer products. The 2B-CLDCLASS-lidar product combines CPR and CALIOP
163 observations to provide cloud top and base heights jointly with cloud thermodynamic phase (ice,
164 liquid or mixed) for each cloud layer; Figure 2 shows an example 2B-CLDCLASS-lidar curtain for
165 a 2008-07-01 data segment starting at 01h 23min. This product provides up to 10 vertical cloud
166 layers at 1km horizontal resolution along-track. Since the upper cloud layer optical thickness is
167 critical in understanding the impact of multilayer cloud scenes on MYD06 cloud optical property
168 retrievals, cloud optical thickness from the CALIOP 5km layer product is merged with the
169 CLDCLASS-lidar product. This is accomplished by re-sampling the CALIOP product at 1km and
170 searching for matching cloud layers between the CALIOP 5km and 2B-CLDCLASS-lidar 1km
171 cloud layer products. Collocated files of MODIS and 2B-CLDCLASS-lidar have also been created
172 containing the pixel indices of 2B-CLDCLASS-lidar and the nearest MODIS pixel in terms of
173 spatial distance in the geographic coordinate system.



174

175 **IV - Evaluation of the MYD06 C6.1 multilayer cloud detection algorithm**

176

177 The global performance of the MYD06 multilayer cloud detection algorithm is shown in
178 Figure 3. Here, contingency tables comparing MYD06 multilayer classification results to those
179 from the 2B-CLDCLASS-lidar products are shown when the PH04 test is (a) included and (b)
180 excluded. Note that, for the 2B-CLDCLASS-lidar products, we use a naïve definition of multilayer
181 clouds here, namely all profiles where the merged product indicates more than one cloud layer
182 regardless of layer phase, optical thickness, or separation distance. Several conclusions can be
183 inferred from these tables. First, for the cloudy pixel population for which the MYD06 multilayer
184 detection algorithm is not applied (cloud optical thickness < 4 , top rows), the 2B-CLDCLASS-lidar
185 product indicates a quite high percentage of multilayer clouds, 16.58% of the total cloudy
186 population. As we will show in the next section, this imposed multilayer detection limit in MYD06
187 can impact cloud effective radius retrieval statistics. For the cloudy pixel population for which the
188 MYD06 multilayer detection algorithm is applied (cloud optical thickness > 4 , middle and bottom
189 rows), the MYD06 results including the PH04 test agree with the 2B-CLDCLASS-lidar monolayer
190 and multilayer classifications 33.73% of the time (21.29% for monolayer, 12.44% for multilayer),
191 and disagree 20.04% of the time (12.25% false multilayer detection rate, 7.79% false monolayer
192 detection rate). When the PH04 test is not included, the agreement and disagreement
193 percentages remain roughly the same, 34.95% and 18.83%, respectively, though the
194 apportionment between true/false mono/multilayer detection changes.

195

196 While it is evident in Figure 3 that MYD06 misses a relatively large percentage of multilayer
197 clouds that the radar/lidar merged product detects (7.79% or 11.40% when the PH04 test is
198 included or excluded, respectively), the active sensors are much more capable at detecting



199 multilayer cloud scenes than MODIS. More importantly, as we will see in the next section, in many
200 cases these missed multilayer scenes do not adversely impact the optical property retrieval
201 statistics and are thus beyond the intent of the algorithm. It is therefore important to evaluate the
202 algorithm's performance as a function of two parameters directly related to its intended targets,
203 namely the optical thickness of the upper layer cloud and the vertical separation distance of the
204 cloud layers.

205

206 To better understand the multilayer cloud scenes, we focus on multilayer cloud scenes with
207 only two cloud layers (which represent about 77% of the multilayer cloud population in our co-
208 located dataset). Figure 4 shows the probability that MYD06 correctly identifies a multilayer cloud,
209 using the 2B-CLDCLASS-lidar data as truth, given the separation distance d (the distance
210 between the cloud base of the upper cloud and the cloud top of the bottom cloud) and the upper
211 layer cloud optical thickness τ defined by the CALIOP 5km cloud layer products. Results are
212 shown when including (a) and excluding (b) the PH04 test. Note that all 2B-CLDCLASS-lidar
213 multilayer cloud scenes are included in the baseline here regardless of layer thermodynamic
214 phase. One can see, from Figure 4a, that the PH04 test is very sensitive to multilayer clouds,
215 even if d and τ are quite small, but at the expense of a larger false positive rate (see Figure 3a).
216 On the other hand, if the PH04 test is not used (Figure 4b), one can see that the probability of
217 correctly detecting a multilayer cloud scene increases with both d and τ . Regardless of the
218 inclusion of the PH04 test, however, the results shown here indicate that it is probable that MYD06
219 will detect a multilayer cloud if the separation distance d is greater than 1km and the upper layer
220 cloud optical thickness is greater than about 1.2.

221



222 In addition to cloud layer detection, the 2B-CLDCLASS-lidar products also provide a cloud
223 thermodynamic phase classification, i.e., liquid, ice or mixed phase, for each detected cloud layer
224 that can be used to evaluate the performance of the MYD06 cloud optical properties phase
225 algorithm in multilayer scenes. Note that the C6/C6.1 MOD06/MYD06 phase algorithm was tuned
226 and validated against the CALIOP 1 and 5 km cloud layer products using two months of collocated
227 data, though only for scenes where CALIOP observed only a single phase in the profile (Marchant
228 et al., 2016). Figure 5a shows a similar single-phase validation using the 2B-CLDCLASS-lidar
229 products for monolayer clouds only with a single cloud phase in 2008. While agreement for liquid
230 and ice phase results is 65.22%, 26.62% of 2B-CLDCLASS-lidar monolayer clouds are identified
231 as mixed phase, of which MYD06 identifies 9.85% and 16.77% as ice and liquid phase,
232 respectively.

233

234 Extending this monolayer analysis to multilayer cloud scenes, two types of multilayer cases
235 can be distinguished in the 2B-CLDCLASS-lidar product, namely profiles where the multiple cloud
236 layers share the same thermodynamic phase and those where they do not. Figure 5b shows the
237 comparison between the MYD06 cloud optical properties phase and the 2B-CLDCLASS-lidar
238 product for two cloud layers sharing the same cloud phase (roughly 10% of the co-located
239 dataset). When 2B-CLDCLASS-lidar identifies two ice layers or two liquid layers in the profile, the
240 MYD06 phase agrees 82.57% of the time. However, in 12.06% of the multilayer cases, MYD06
241 misidentifies an ice cloud overlapping another ice cloud as liquid cloud phase.

242

243 Figure 6 shows phase comparison results for the cases where 2B-CLDCLASS-lidar
244 identifies two cloud phases in the vertical profile (roughly 20% of the co-located dataset). The
245 most frequent cloud scene is an ice cloud overlapping a liquid cloud (59.54% of these cases, first
246 column), for which MYD06 identifies fractions of 27.27% ice and 32.27% liquid clouds. For ice



247 clouds overlapping mixed phase clouds, the second most frequent scene (30.74% of these cases,
248 second column), MYD06 is more likely to identify ice phase (16.45%) rather than liquid phase
249 (14.29%).

250

251 The ambiguity of the results in Figure 6 underscores the difficulty of determining a single
252 phase in a multilayer scene using MODIS when there is no unique answer on the true column
253 phase. Moreover, because the MYD06 cloud optical properties phase is a radiatively derived
254 designation, it must depend on, for example, the upper layer cloud optical thickness and the
255 sun/satellite viewing geometry. Focusing only on the case of ice clouds overlapping liquid clouds,
256 Figure 7 shows the probability that MYD06 (a) correctly identifies a multilayer cloud (PH04 test
257 excluded), and the probabilities of (b) undetermined, (c) ice, and (d) liquid phase results, each as
258 a function of layer separation distance d and upper layer cloud optical thickness τ . The probability
259 that MYD06 correctly identifies an ice cloud overlapping a liquid cloud as multilayer (Fig. 7a) is
260 similar in pattern to the probabilities for all multilayer scenes regardless of the cloud layer phase
261 in Figure 4b, though the magnitude of the probabilities here is larger. The MYD06 phase result
262 probabilities (Fig. 7b-d) are largely what one would expect, in particular that the probability of an
263 ice cloud result increases as the upper ice cloud optical thickness increases, while the probability
264 of a liquid cloud result shows the opposite pattern; the probability of an undetermined phase result
265 is largest when the two cloud layers are vertically close and the upper layer cloud optical thickness
266 is greater than 0.7.

267

268 **V - Assessing the MYD06 multilayer cloud flag as an optical property retrieval quality**
269 **indicator**

270



271 Given the intent of the MOD06/MYD06 multilayer cloud detection algorithm, namely to
272 identify scenes that do not conform to the single-layer cloud forward model assumption, we
273 assess the utility of the multilayer algorithm's results as a QA tool for the cloud optical property
274 retrievals. In particular, we focus on cloud effective radius retrievals, where multilayer scenes are
275 expected to have retrieval artifacts or uninterpretable results due to the mixing of particle
276 scattering properties from multiple cloud layers having different phases and/or microphysics. To
277 facilitate the analysis, we again use the collocated MYD06 and 2B-CLDCLASS-lidar 2008 dataset,
278 and consider two cloudy pixel populations: (1) a reference population containing only monolayer
279 clouds as determined by the 2B-CLDCLASS-lidar product for which the cloud thermodynamic
280 phase is in agreement with that of MYD06; (2) a population of multilayer clouds, defined as those
281 for which the 2B-CLDCLASS-lidar product identifies more than one cloud layer regardless of the
282 cloud layer separation distance, the upper layer cloud optical thickness, or the cloud
283 thermodynamic phase.

284

285 Figure 8 presents the results for liquid (left column) and ice (right column) clouds for the
286 three primary cloud effective radius retrievals reported in the MYD06 cloud optical products,
287 namely those associated with three particle absorptive bands at 2.1, 1.6 and 3.7 μm . One can see
288 the differences between the monolayer cloud (blue) and multilayer cloud (red) populations, and
289 that the ice cloud effective radius populations exhibit the largest differences. In particular, the ice
290 cloud effective radius distributions for the multilayer cloud population have a secondary mode at
291 effective radius around 10-15 μm . This secondary mode can be explained by a large fraction of
292 cases in the co-located dataset having ice overlapping liquid clouds (see Figure 6, left column).
293 Since liquid droplets are less absorptive than ice crystals in these spectral channels for a given
294 size, identifying these scenes as ice phase can yield smaller ice cloud effective radius retrievals.
295 Indeed, if we remove from the multilayer population those cloudy pixels classified by MYD06 as



296 multilayer, as shown in Figure 9 for cases where MYD06 cloud optical thickness exceeds 4, one
297 can see that the secondary peaks in the ice effective radius distributions for multilayer clouds
298 (red) have disappeared. Therefore, though the MYD06 multilayer cloud detection is not able to
299 detect all multilayer clouds, it can be used to filter cloud effective radius retrievals that are
300 radiatively impacted by multilayer cloud scenes. Even if the PH04 algorithm is ignored in the
301 MYD06 multilayer cloud detection algorithm (Figure 10), the multilayer detection results remain
302 useful for removing most of the differences between the two populations, though some portion of
303 the small ice cloud effective radii remain.

304

305 If the MODIS cloud optical thickness is lower than 4, the multilayer cloud detection algorithm
306 is not applied since forward modeling indicated that there is not enough information to discriminate
307 monolayer and multilayer clouds (Wind et al. 2010). Figure 11 shows, however, that some
308 noticeable differences remain in the MODIS cloud effective radius distributions for monolayer and
309 multilayer clouds as determined by the 2B-CLDCLASS-lidar products. It is then not possible to
310 directly screen out the cloud effective radius strongly biased by the presence of multilayer cloud
311 scenes as we showed previously.

312

313 **VI – Conclusions**

314

315 In an evaluation of the MODIS multilayer cloud detection algorithm by comparing Aqua
316 MODIS MYD06 C6.1 with a merged CPR and CALIOP products, . As expected, the results are
317 quite sensitive to the definition of a multilayer cloud scene for active sensor products. Therefore,
318 three main parameters have been used to defined a multilayer cloud scene: (1) the maximum
319 separation distance d between the two cloud layers, (2) the thermodynamic phase of those layers,
320 and (3) the upper layer optical thicknesses. Overall, the global MODIS multilayer cloud detection



321 algorithm skill performs well when the optical thickness of the upper layer is greater than about 1-
322 2 and the separation distance d is greater than 1km. In parallel, the impact of using a $1.38 \mu\text{m}$
323 channel in a multilayer algorithm (PH04, Pavolonis and Heidinger, 2004) was studied; PH04 was
324 added as a separate test to the MODIS multilayer algorithm beginning with Collection 6. It was
325 found that this algorithm flags too many cloudy scenes as multilayer, leading to an increase in
326 false positive occurrences, i.e. cloudy pixels wrongly flagged as multilayer.

327 This study also allowed for an expanded evaluation of the MODIS cloud
328 thermodynamic phase (Marchant et al. 2016), that was based on single layer CALIOP
329 observations, to the more general case of multilayer cloud scenes. For monolayer clouds, the
330 current analysis based on CPR and CALIOP gives results similar to Marchant et al. (which used
331 a different time period) in terms of showing a phase agreement fraction of about 91%. For two
332 spatially separated cloud layers detected by the CPR and CALIOP sensors, scenes with the same
333 cloud phase in the two layers were analyzed separately from scenes having different layer
334 phases. When the cloud phase is liquid in both cloud layers, there is good agreement between
335 the MODIS and active sensor cloud phases. When an ice cloud layer overlies another ice layer,
336 the MODIS phase is often retrieved as liquid; further investigation is needed for these cases.
337 When the cloud phase is different in the two cloud layers, the preferred phase for MODIS should
338 be based on the radiative contribution from each layer to the observed signal. For instance, the
339 most frequent cases, according to 2B-CLDCLASS-lidar products, are ice overlying liquid clouds
340 for which the fraction of ice or liquid cloud retrieved by MODIS are about the same but this includes
341 radiatively thin upper cloud layers. MYD06 is more and more likely to identify ice phase rather
342 than liquid phase with the increase of the ice cloud optical thickness.

343

344 Even though the MODIS C6 multilayer cloud detection algorithm is not able to detect all
345 multilayer cloud scenes compared to the merged CPR and CALIOP product (MYD06 results



346 including the PH04 test agree with the 2B-CLDCLASS-lidar monolayer and multilayer
347 classifications 33.73% of the time, disagree 20.04% of the time), the algorithm is reasonably
348 skilled in its intended use, i.e., discriminating those pixels for which the cloud effective radius may
349 be biased by layers having different microphysics (phase and/or effective particle size). MODIS
350 ice phase categorized clouds have effective radius retrievals that are most impacted by multilayer
351 cloud scenes, with a small radius bias. If the PH04 detection algorithm output is not used, the
352 fraction of multilayer clouds flagged by MODIS is smaller but the MODIS multilayer cloud
353 algorithm then has less skill to screen out cloud effective radius impacted by the presence of
354 multilayer clouds. Finally, it was found that when the column cloud optical thickness is less than
355 4, cutoff used by the MODIS algorithm, cloud effective radius retrievals can still be impacted by
356 multilayer clouds identified with the active sensor products. Further work on extending the MODIS
357 multilayer cloud detection algorithm to smaller column cloud optical thicknesses is warranted.

358

359 **V - References**

360

- 361 - Chang, F.-L., Li, Z.: A New Method for Detection of Cirrus Overlapping Water Clouds and
362 Determination of Their Optical Properties. *Journal of the Atmospheric Sciences*, 62(11), 3993–
363 4009. <https://doi.org/10.1175/jas3578.1>, 2005.
- 364 - Cho, H.-M., Zhang, Z., Meyer, K., Lebsock, M., Platnick, S., Ackerman, A. S., Girolamo, L.D. ,
365 Labonnote, L.C., Cornet, C., Riedi, J., E. Holz, R.E.: Frequency and causes of failed MODIS
366 cloud property retrievals for liquid phase clouds over global oceans. *Journal of Geophysical*
367 *Research: Atmospheres*, 120(9), 4132–4154. <https://doi.org/10.1002/2015jd023161>, 2015.
- 368 - Desmons, M., Ferlay, N., Parol, F., Riédi, J., Thieuleux, F.: A Global Multilayer Cloud
369 Identification with POLDER/PARASOL. *Journal of Applied Meteorology and Climatology*, 56(4),
370 1121–1139. <https://doi.org/10.1175/jamc-d-16-0159.1>, 2017.



- 371 - Heidinger, A. K., Pavolonis, M. J.: Global Daytime Distribution of Overlapping Cirrus Cloud
372 from NOAA's Advanced Very High-Resolution Radiometer. *Journal of Climate*, 18(22), 4772–
373 4784. <https://doi.org/10.1175/jcli3535.1>, 2005.
- 374 - Jin, Y., Rossow, W. B.: Detection of cirrus overlapping low-level clouds. *Journal of Geophysical*
375 *Research: Atmospheres*, 102(D2), 1727–1737. <https://doi.org/10.1029/96jd02996>, 1997.
- 376 - Joiner, J., Vasilkov, A. P., Bhartia, P. K., Wind, G., Platnick, S., Menzel, W. P.: Detection of
377 multi-layer and vertically-extended clouds using A-train sensors. *Atmospheric Measurement*
378 *Techniques*, 3(1), 233–247. <https://doi.org/10.5194/amt-3-233-2010>, 2010.
- 379 - Li, J., Huang, J., Stamnes, K., Wang, T., Lv, Q., Jin, H.: A global survey of cloud overlap based
380 on CALIPSO and CloudSat measurements. *Atmospheric Chemistry and Physics*, 15(1), 519–
381 536. <https://doi.org/10.5194/acp-15-519-2015>, 2015.
- 382 - Marchant, B., Platnick, S., Meyer, K., Arnold, G. T., Riedi, J.: MODIS Collection 6 shortwave-
383 derived cloud phase classification algorithm and comparisons with CALIOP. *Atmospheric*
384 *Measurement Techniques*, 9(4), 1587–1599. <https://doi.org/10.5194/amt-9-1587-2016>, 2016.
- 385 - Nasiri, S. L., Baum, B. A.: Daytime Multilayered Cloud Detection Using Multispectral Imager
386 Data. *Journal of Atmospheric and Oceanic Technology*, 21(8), 1145–1155.
387 [https://doi.org/10.1175/1520-0426\(2004\)021<1145:dmcdum>2.0.co;2](https://doi.org/10.1175/1520-0426(2004)021<1145:dmcdum>2.0.co;2), 2004.
- 388 - Pavolonis, M. J., Heidinger, A. K.: Daytime Cloud Overlap Detection from AVHRR and VIIRS.
389 *J. Appl. Meteorology*, 43, 762-778, doi:10.1175/2099.1, 2004.
- 390 - Platnick, S., Meyer, K. G., King, M. D., Wind G., Amarasinghe N., Marchant B., Arnold G.T.,
391 Zhang Z., Hubanks P. A., Holz R.E., Yang P., Ridgway W. L., Riedi, J.: Te MODIS cloud optical
392 and microphysical products: Collection 6 updates and examples from Terra and Aqua. *IEEE*
393 *Trans. Geosci. Remote Sens.*, 55, 502-525, 2017.



- 394 - Sassen, K., Wang, Z., Liu, D.: Global distribution of cirrus clouds from CloudSat/Cloud-Aerosol
395 Lidar and Infrared Pathfinder Satellite Observations (CALIPSO) measurements. Journal of
396 Geophysical Research, 113. <https://doi.org/10.1029/2008jd009972>, 2008.
- 397 - Sourdeval, O., C.-Labonnote, L., Baran, A. J., Brogniez, G.: A methodology for simultaneous
398 retrieval of ice and liquid water cloud properties. Part I: Information content and case study.
399 Quarterly Journal of the Royal Meteorological Society, 141(688), 870–882.
400 <https://doi.org/10.1002/qj.2405>, 2014.
- 401 - Sourdeval, O., C.-Labonnote, L., Baran, A. J., Mülmenstädt, J., Brogniez, G.: A methodology
402 for simultaneous retrieval of ice and liquid water cloud properties. Part 2: Near-global retrievals
403 and evaluation against A-Train products. Quarterly Journal of the Royal Meteorological Society,
404 142(701), 3063–3081. <https://doi.org/10.1002/qj.2889>, 2016.
- 405 - Vitter, J. S.: Random sampling with a reservoir. ACM Transactions on Mathematical Software,
406 11(1), 37–57. <https://doi.org/10.1145/3147.3165>, 1985.
- 407 - Wang, T., Fetzer, E. J., Wong, S., Kahn, B. H., Yue, Q.: Validation of MODIS cloud mask and
408 multilayer flag using CloudSat-CALIPSO cloud profiles and a cross-reference of their cloud
409 classifications. Journal of Geophysical Research: Atmospheres, 121(19), 11,620–11,635.
410 <https://doi.org/10.1002/2016jd025239>, 2016.
- 411 - Wang, Z., Vane D., Stephens G., Reinke D. Level 2 Combined Radar and Lidar Cloud Scenario
412 Classification Product Process Description and Interface Control Document
413 <http://www.cloudsat.cira.colostate.edu/sites/default/files/products/files/2B-CLDCLASS->
414 [LIDAR_PDICD.P_R04.20120522.pdf](http://www.cloudsat.cira.colostate.edu/sites/default/files/products/files/2B-CLDCLASS-LIDAR_PDICD.P_R04.20120522.pdf)
- 415 - Watts, P. D., Bennartz, R., Fell, F.: Retrieval of two-layer cloud properties from multispectral
416 observations using optimal estimation. Journal of Geophysical Research, 116(D16).
417 <https://doi.org/10.1029/2011jd015883>, 2011.



418 - Wind, G., Platnick, S., King M.D., Hubanks, P.A., Pavolonis, M.J., Heidinger, A.K., Yang P.,
419 Baum, B.A.: “Multilayer Cloud Detection with the MODIS Near-Infrared Water Vapor Absorption
420 Band.” Journal of Applied Meteorology and Climatology 49 11 (November): 2315–2333.
421 doi:10.1175/2010jamc2364.1. <http://dx.doi.org/10.1175/2010JAMC2364.1>, 2010.

422
423
424

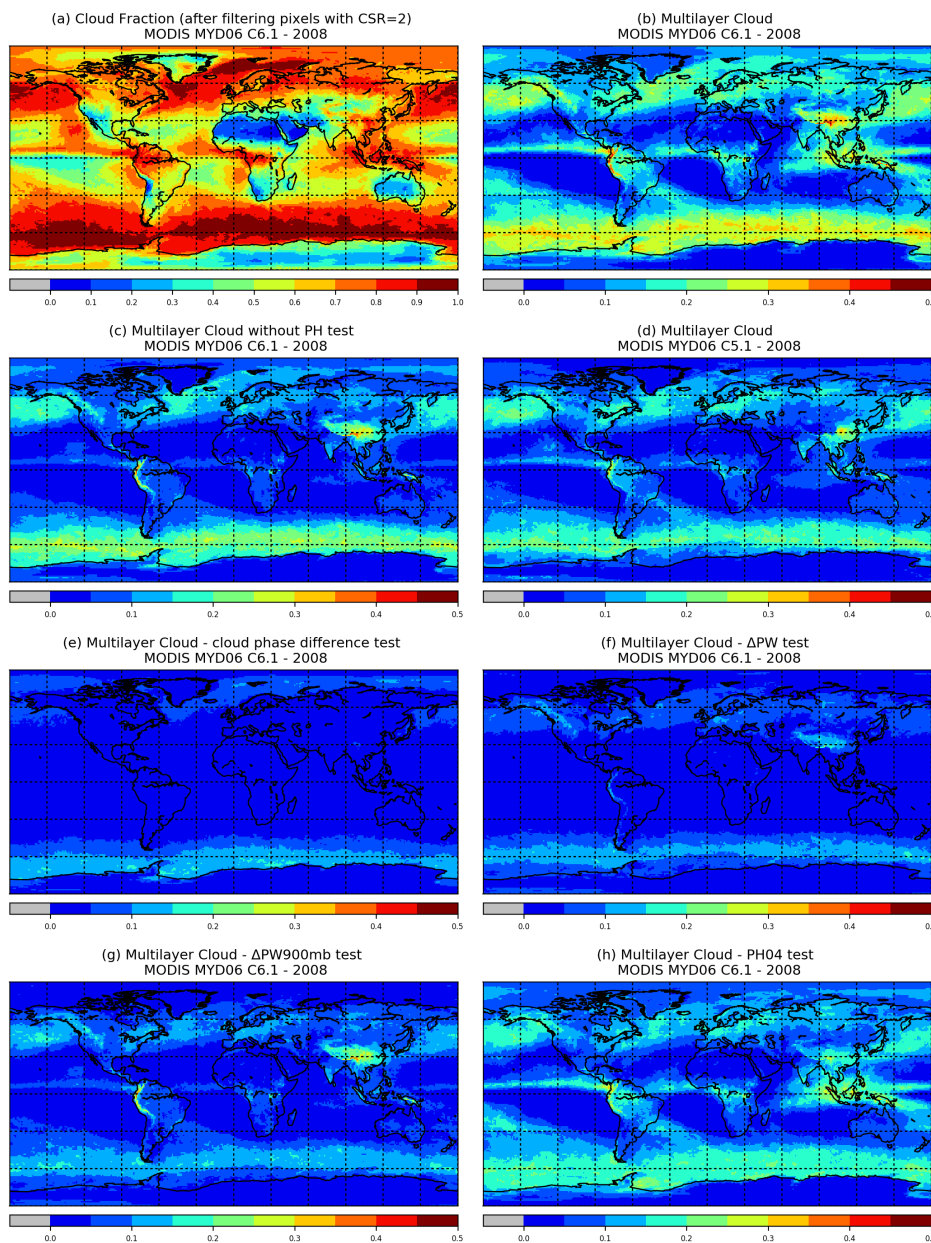


Figure 1: A collection of aggregated (all pixel) Aqua MODIS Level 2 cloud products over the year 2008: (a) cloud fraction, (b) C6.1 multilayer cloud fraction, (c) C6.1 multilayer cloud fraction excluding the Pavolonis and Heidinger (2004) (PH04) test, and (d) C5.1 multilayer cloud fraction; fractions determined from each individual C6.1 multilayer cloud detection test: (e) cloud phase difference test, (f) ΔPW test (g) ΔPW_{900mb} test, and (h) PH04 test.



426
427
428
429
430
431
432
433

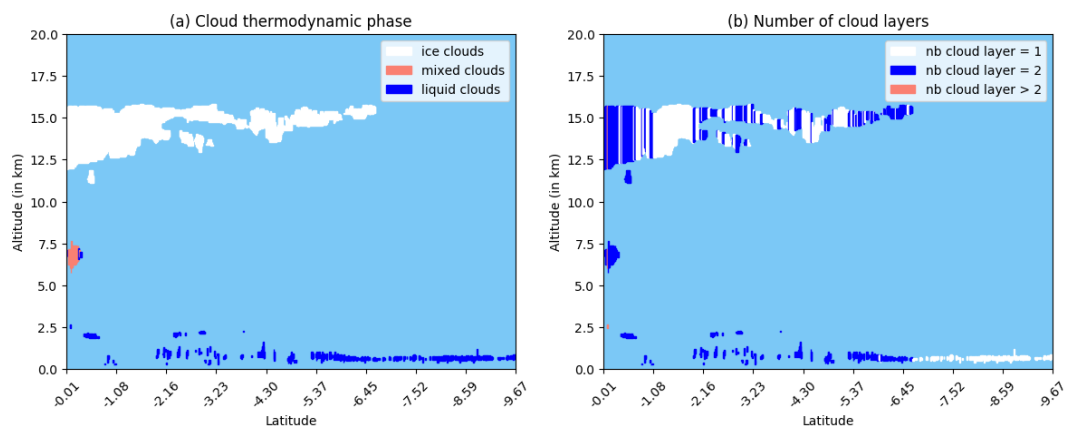


Figure 2: An example 2B-CLDCLASS-lidar curtain (2008183012329_11573_CS_2B-CLDCLASS-LIDAR_GRANULE_P_R04_E02.hdf): (a) cloud thermodynamic phase for each detected cloud layer (ice, liquid or mixed); (b) the number of cloud layers found after merging cloud layers with a vertical separation distance less than 3km.

434
435
436
437
438
439



440
 441
 442
 443
 444
 445
 446

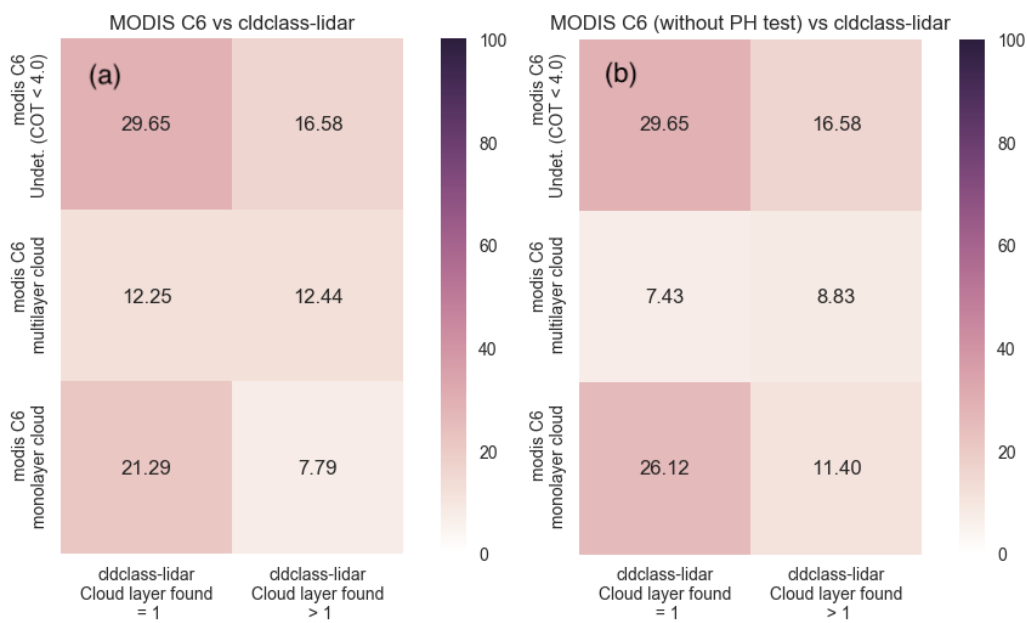


Figure 3: Contingency tables of the MYD06 C6.1 multilayer cloud detection algorithm compared against multilayer clouds defined by the 2B-CLDCLASS-lidar products: MYD06 (a) with and (b) without the Pavlonis-Heidinger (PH04) test. The 2B-CLDCLASS-lidar multilayer clouds are defined regardless of the separation distance between the cloud layers, the cloud thermodynamic phase or the cloud optical thickness.

447
 448
 449
 450



451

452

453

454

455

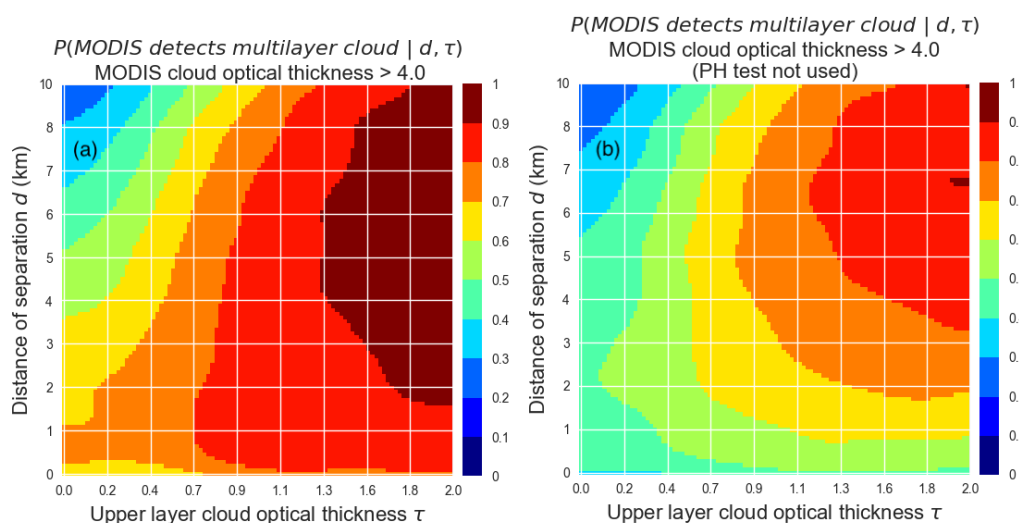


Figure 4: Probabilities that MYD06 detects a multilayer cloud, (a) with and (b) without the Pavolonis-Heidinger (PH04) test, given the separation distance between two cloud layers and the cloud optical thickness of the upper layer derived from 2B-CLDCLASS-lidar and CALIOP 5km cloud products, respectively.

456

457

458

459

460

461

462

463



464
 465
 466
 467
 468

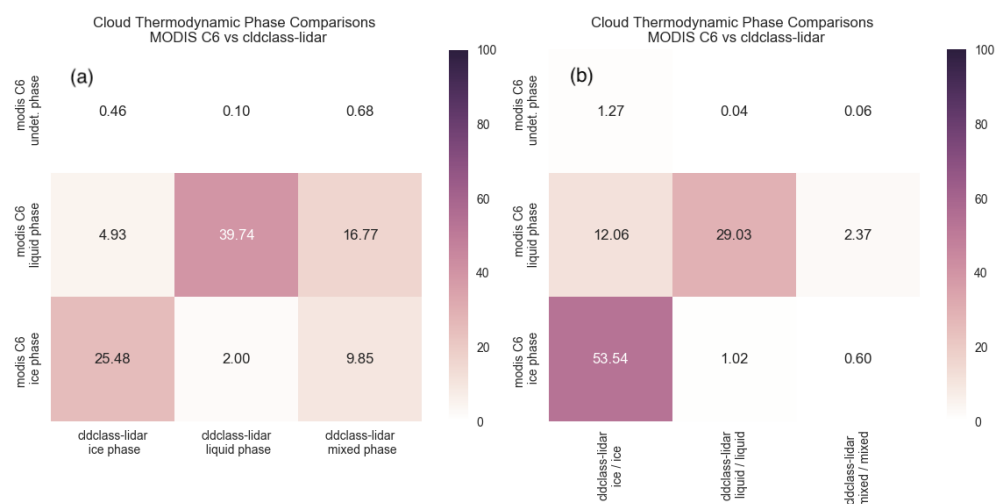


Figure 5: MYD06 C6.1 cloud thermodynamic phase compared to 2B-CLDCLASS-lidar cloud phase: (a) monolayer clouds (about 63% of the dataset), and (b) multilayer clouds having the same phase (about 10% of the co-located dataset). Here, mono/multilayer clouds are defined by 2B-CLDCLASS-lidar.

469
 470
 471
 472
 473
 474
 475
 476



477
 478
 479
 480
 481
 482
 483

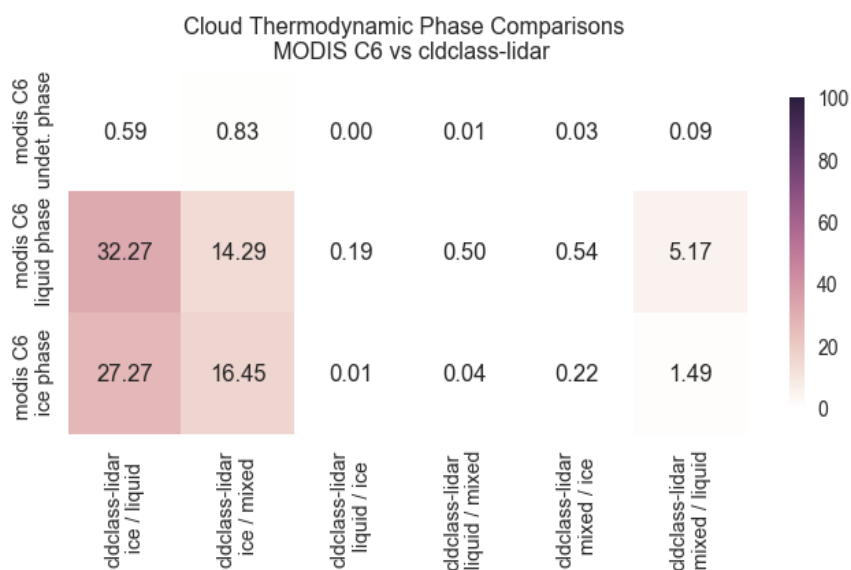


Figure 6: MYD06 C6.1 cloud optical properties thermodynamic phase compared to 2B-CLDCLASS-lidar cloud phase for multilayer clouds having a different cloud phase in the vertical profile. “Ice/liquid” refers to an upper ice layer overlying a liquid cloud layer, and similarly for other notions (about 20% of the co-located dataset).

484
 485
 486
 487



488

489

490

491

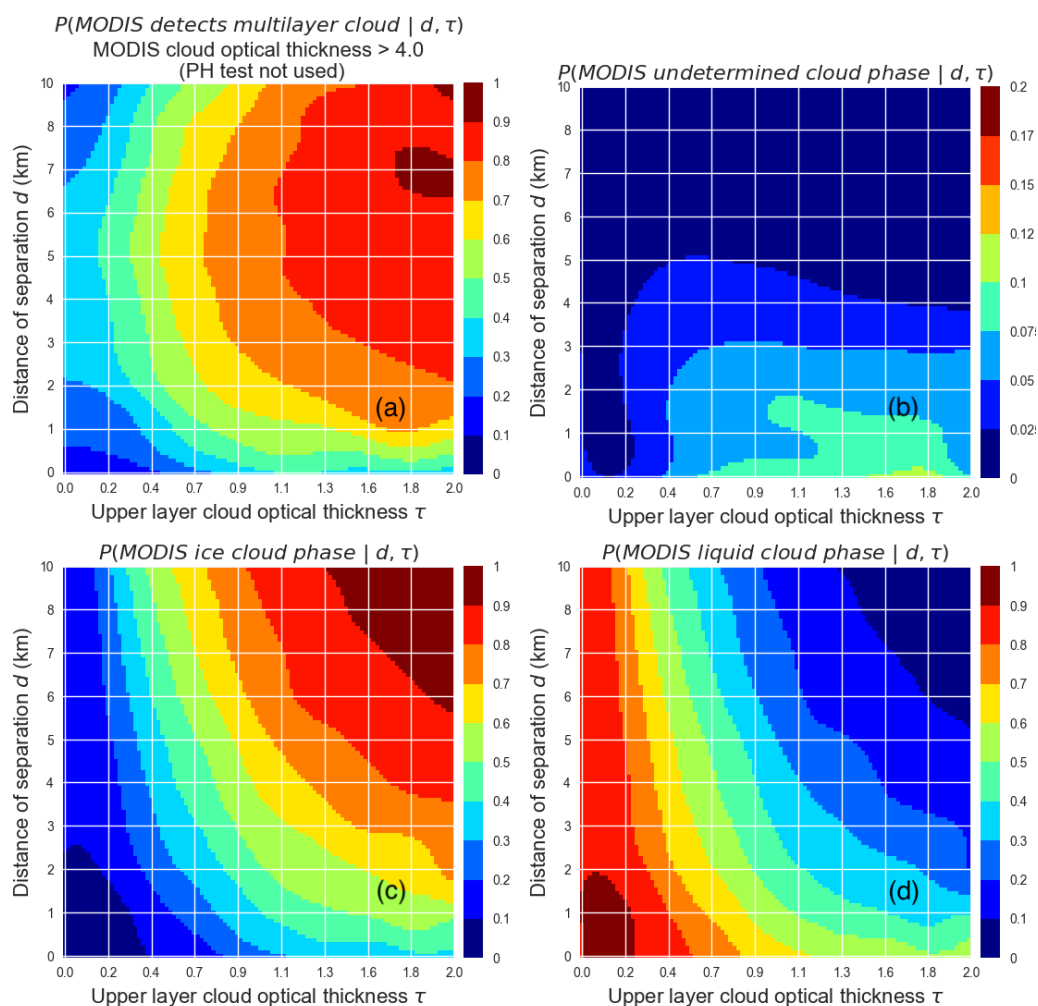


Figure 7: (a) Probability that the MYD06 multilayer cloud detection algorithm detects an ice cloud overlapping a liquid cloud (with the PH test turned off) given the separation distance “ d ” between the two cloud layers and the upper layer cloud optical thickness “ τ ” defined by the 2B-CLDCLASS-lidar products; probabilities that the MYD06 cloud optical properties phase algorithm provides an undetermined (b), ice (c) or liquid (d) cloud phase given “ d ” and “ τ ”.



492

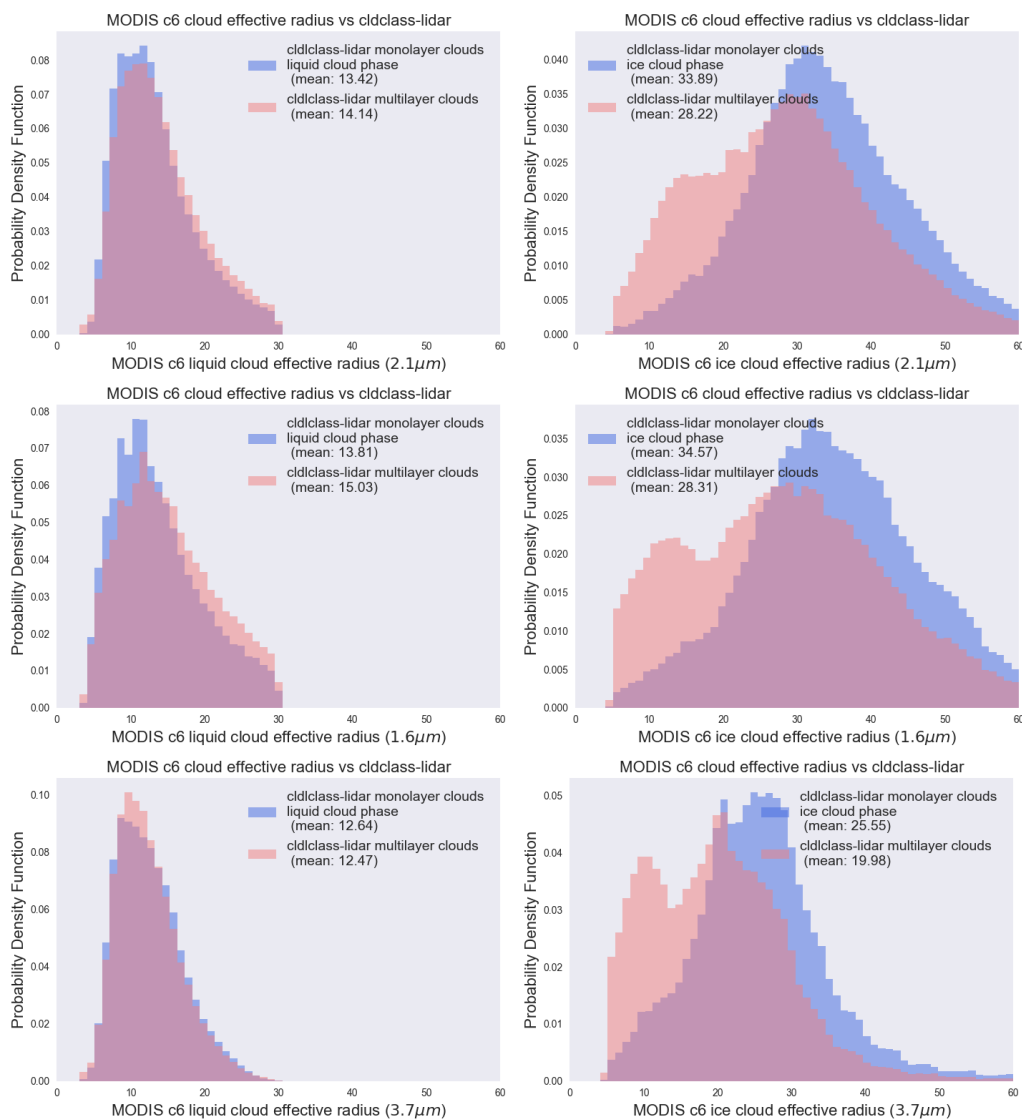


Figure 8: MYD06 1.6, 2.1, 3.7 μm liquid (left column) and ice (right column) cloud effective radius retrieval distributions for monolayer (light blue) and multilayer (light red) cloud populations as determined by the 2B-CLDCCLASS-lidar products regardless of the cloud layer separation distance or the upper layer cloud optical thickness.

493

494



495

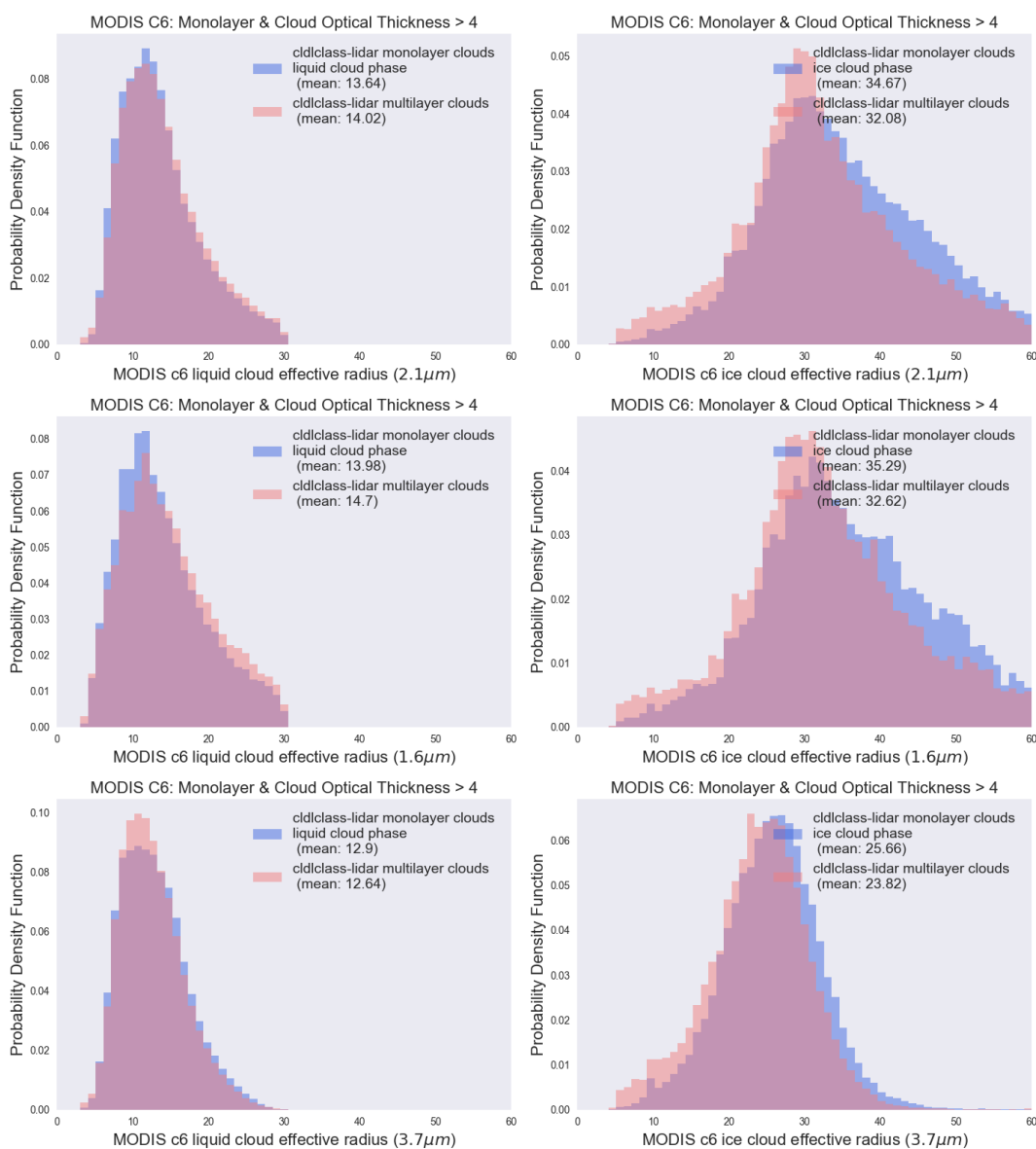


Figure 9: Same as Figure 8, but for the population having MYD06 cloud optical thickness larger than 4 and after removing from the multilayer cloud population (in red) the cloudy pixels classified by the MYD06 multilayer cloud detection algorithm as multilayer clouds.

496



497

498

499

500

501

502

503

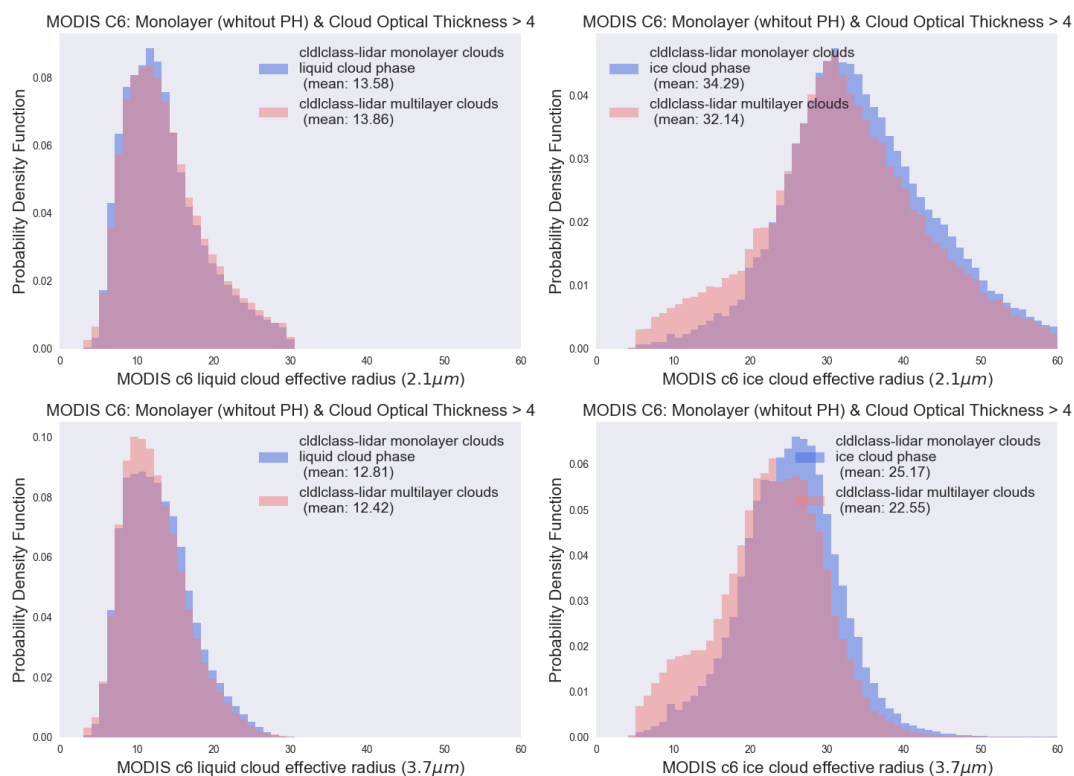


Figure 10: Same as Figure 9, but excluding the Pavlonis and Heidinger detection algorithm in the MYD06 multilayer cloud detection algorithm.

504

505

506



507

508

509

510

511

512

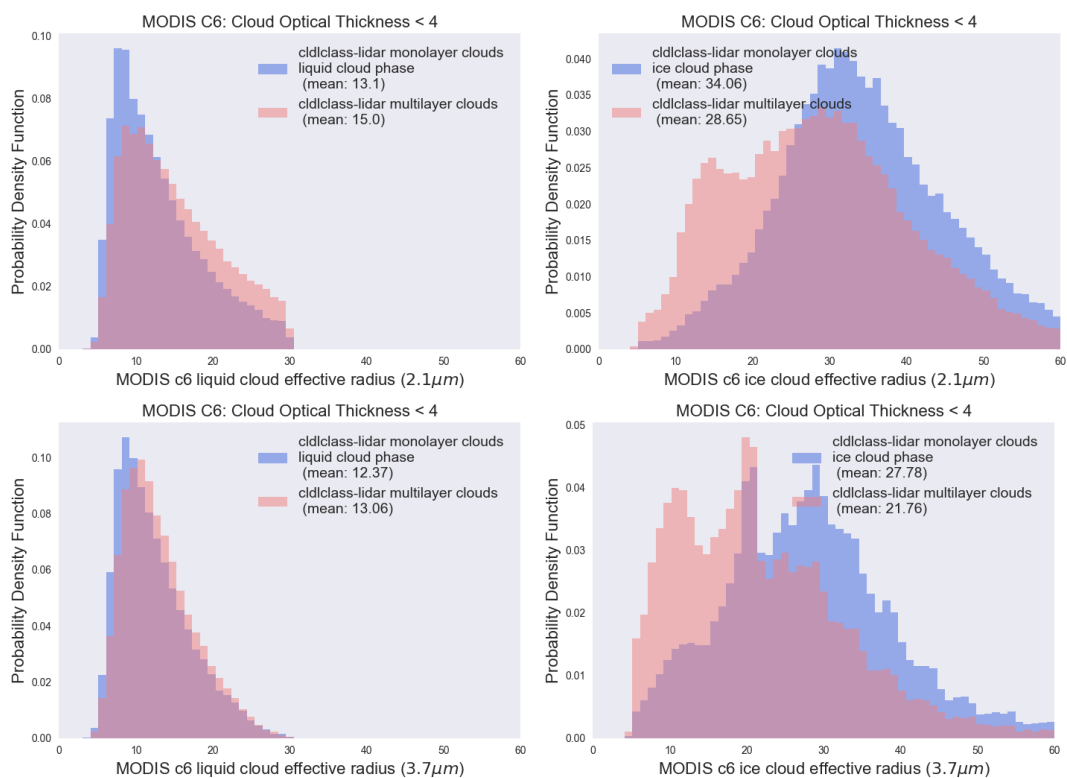


Figure 11: Differences in MYD06 cloud effective radius distributions for monolayer (in blue) and multilayer (in red) clouds for the population having MYD06 cloud optical thickness lower than 4.

513

514

515